THE JOURNAL OF PHYSICAL CHEMISTRY B
A JOURNAL OF THE AMERICAN CHEMICAL SOCIETY

pubs.acs.org/JPCB

Article

Interfacial Properties of Hydrophobic Deep Eutectic Solvents with Water

Hirad S. Salehi, Othonas A. Moultos, and Thijs J. H. Vlugt*

Cite This: *J. Phys. Chem. B* 2021, 125, 12303−12314

Read Online

ACCESS | Metrics & More | Article Recommendations | Supporting Information

ABSTRACT: Hydrophobic deep eutectic solvents (DESs) have recently gained much attention as water-immiscible solvents for a wide range of applications. However, very few studies exist in which the hydrophobicity of these DESs is quantified. In this work, the interfacial properties of hydrophobic DESs with water were computed at various temperatures using molecular dynamics simulations. The considered DESs were tetrabutylammonium chloride−decanoic acid (TBAC−dec) with a molar ratio of 1:2, thymol−decanoic acid (Thy−dec) with a molar ratio of 1:2, and DL-menthol−decanoic acid (Men−dec) with a molar ratio of 2:1. The following properties were investigated in detail: interfacial tensions, water-in-DES solubilities (and salt-in-water solubilities for TBAC−dec/water), density profiles, and the number densities of hydrogen bonds. Different ionic charge scaling factors were used for TBAC−dec. Thy−dec and Men−dec showed a high level of hydrophobicity with negligible computed water-in-DES solubilities. For charge scaling factors of 0.7 and 1 for the thymol and decanoic acid components of Thy−dec, the computed interfacial tensions of the DESs are in the following order: TBAC−dec (ca. 4 mN m^{-1}) < Thy−dec (20 mN m^{-1}) < Men−dec (26 mN m^{-1}). The two sets of charge scaling factors for Thy−dec did not lead to different density profiles but resulted in considerable differences in the DES/water interfacial tensions due to different numbers of decanoic acid−water hydrogen bonds at the interfaces. Large peaks were observed for the density profiles of (the hydroxyl oxygen of) decanoic acid at the interfaces of all DES/water mixtures, indicating a preferential alignment of the oxygen atoms of decanoic acid toward the aqueous phase.

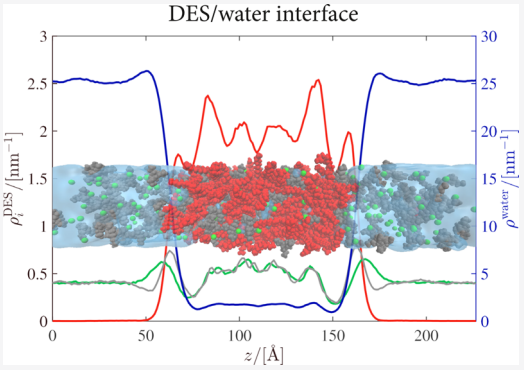

1. INTRODUCTION

Deep eutectic solvents (DESs) are a class of solvents that are considered for a wide range of applications due to favorable properties such as a very small vapor pressure, a low melting point, good solvation for a variety of solutes, easy and cost-efficient preparation, biodegradability, and non-toxicity.[1−6] Most synthesized DESs reported in the literature are hydrophilic.[7] This hydrophilic nature has advantages in applications where DESs are mixed with water or other hydrophilic compounds, such as alcohols, for improved thermophysical properties. However, it limits the use of DESs for applications where the miscibility with water is undesirable, for instance, in liquid−liquid extraction of solutes from aqueous phases.[5,8]

In 2015, van Osch et al.[8] introduced hydrophobic DESs, composed of tetraalkylammonium halide salts and decanoic acid. These DESs were used to extract various fatty acids from water. The authors investigated the influence of the cation alkyl chain lengths on the properties and extraction efficiencies of the DESs. It was shown that the alkyl chain length directly determines the hydrophobicity and the amount of leaching of the DES constituents (in this case cations and anions) to the water phase and consequently the suitability of the DES for the extraction process. Since their introduction in 2015, a growing number of hydrophobic DESs have been synthesized and proposed for a variety of applications, such as CO_2 capture,[9−11] extraction of components from plants,[12,13] extraction of metal ions,[14−16] antibiotics,[17] pesticides,[18] and sugar-based molecules[19,20] from aqueous solutions, and catalysis.[21] The reported DESs are mostly mixtures of hydrophobic hydrogen bond donor (HBD) and hydrogen bond acceptor (HBA) components in a specific molar ratio. Charge neutral as well as charged molecules (salts containing cations and anions) may be used in hydrophobic DESs.[22]

So far, hydrophobic DESs have been mostly studied from an application standpoint. For a systematic design of solvents for applications, knowledge on the molecular/atomic-level interactions and structure−property relationships is crucial. Particularly for hydrophobic DESs, theoretical studies of DES/water interfaces at the nanoscale and the quantification

Received: September 2, 2021
Revised: October 19, 2021
Published: October 31, 2021

https://doi.org/10.1021/acs.jpcb.1c07796
J. Phys. Chem. B 2021, 125, 12303−12314

of the hydrophobicity are of utmost importance for the design of optimal extractants as well as interface modifiers. Molecular dynamics (MD) is a powerful tool that has been widely used to study the thermodynamic and structural properties of aqueous solutions of hydrophilic DESs.[23−31] Several MD studies investigating the interfacial properties of biphasic systems of hydrophobic ionic liquids (ILs) and water are also available.[32−39] In sharp contrast to this, very limited studies are available exploring the properties of mixtures of hydrophobic DESs with water using MD simulations.[40−42] Verma et al.[40] studied the extraction efficiency of alcohols from aqueous solutions using menthol-based DESs. These authors computed a variety of properties, such as radial distribution functions (RDFs), diffusion coefficients, and interaction energies of the DES−alcohol−water ternary systems. Paul et al.[41] investigated the stability of several hydrophobic DESs in the presence of water and computed structural properties, such as hydrogen bond populations and RDFs, as well as self-diffusivities in the water−DES mixtures. The authors further investigated the efficiency of extraction of the pesticide nitenpyram from water using menthol−octanoic acid DES and concluded that this DES is a suitable extractant for this process. In a very recent study, Paul et al.[42] computed structural properties of biphasic systems of water and the lidocaine−oleic acid DES as well as dynamical properties (e.g., dipole autocorrelation function) of water in these systems at various temperatures in order to understand the phase segregation mechanism above the lower critical solution temperature.

In this work, interfacial properties of several hydrophobic DESs with water were studied using MD simulations. The DESs were composed of tetrabutylammonium chloride (TBAC), thymol, or DL-menthol (racemic mixture of enantiomers D-menthol and L-menthol) as the HBA component and decanoic acid as the HBD component and are denoted by "tetrabutylammonium chloride−decanoic acid (TBAC−dec)", "thymol−decanoic acid (Thy−dec)", and "DL-menthol−decanoic acid (Men−dec)", respectively. HBA/HBD molar ratios of 1:2, 1:2, and 2:1 were used in the simulations of the TBAC−dec/water, Thy−dec/water, and Men−dec/water systems, respectively. The density profiles of various species in the direction perpendicular to the interface were computed from MD trajectories. To quantify the hydrophobicity of the DESs, the mutual solubilities of DES and water (from the obtained density profiles) and the interfacial tensions were computed for each DES/water system. The effect of charge scaling factor on the computed properties was investigated as this parameter has been shown to significantly influence the properties of ILs and DESs.[34,43−48] A hydrogen bond analysis was performed to investigate the interactions of the various mixture components, which result in the computed interfacial tensions and density profiles.

This article is organized as follows: in the following section, the force field parameters and computational methods are discussed. Subsequently, the simulation results are discussed and compared with the available data from the literature. Finally, conclusions are provided regarding the computation of interfacial properties of hydrophobic DESs with water.

2. COMPUTATIONAL DETAILS

The generalized AMBER force field (GAFF)[49] was used to model the intramolecular and intermolecular interactions of the DESs. The bonded terms of the force field consisted of bond stretching, bond bending, torsions, and improper torsions, and the non-bonded terms consisted of the Lennard-Jones (LJ) and electrostatic energies. The LJ parameters of Fox and Kollman[50] were used for the chloride ion. The electrostatic potential was computed for optimized geometries of isolated molecules/ions at the HF/6-31G* level of theory. The partial charges were obtained from the electrostatic potential using the restrained electrostatic potential method.[51] The Gaussian 09 Rev.B.01 software[52] and the R.E.D-III.52 tools[53] were used to optimize molecular geometries and obtain the electrostatic potential and charges. In our previous work,[46] the force field parameters were validated for neat TBAC−dec. In that study, a charge scaling factor, f_q, of 0.6 for the cation and anion (the HBA component) resulted in more accurate densities and shear viscosities compared to experimental data by van Osch et al.[8] To investigate the effect of charge scaling on the DES/water interfacial properties, different charge scaling values (0.6−0.9) were used for the HBA component of TBAC−dec, that is, the TBAC salt. For simplicity, we did not try to fit a unique scaling factor that is applicable to all the DESs in this study. For Men−dec and Thy−dec, the force field parameters were validated by computing the densities and shear viscosities of the pure DESs and comparing the results with experimental data available in the literature.[54,55] Based on these results, the optimal charge scaling factors were chosen for Men−dec and Thy−dec DESs. For all DESs, the 1−4 intramolecular LJ and electrostatic energies were scaled by 0.5 and 0.833, respectively, according to the GAFF force field.[49] To compute the LJ interactions between non-identical atom types, the Lorentz−Berthelot mixing rules[56] were used. The SPC/E model[57] was used for water. The SHAKE algorithm[56,58] was used to keep the bond lengths and angles of the water molecules fixed. To prevent atomic overlaps, the LJ parameters ε = 0.001 kcal mol^{-1} and σ = 0.1 Å were used for unprotected hydroxyl hydrogen atoms in DES and water molecules. The structures and force field parameters for all the molecules are provided in Supporting Information. The velocity Verlet algorithm[59−61] was used to integrate the equations of motion with a timestep of 1 fs. A Nosé−Hoover thermostat and barostat[59] were used to impose the temperature and pressure, respectively. The barostat was only applied in the direction perpendicular to the interface, thus only changing the simulation box length in this direction. Periodic boundary conditions were used in all three dimensions. All simulations were performed with the LAMMPS software (version 16 March 2018),[62] and the initial configurations were generated using the PACKMOL package.[63] The VMD software[64] was used to visualize the snapshots of the systems.

In all simulations, a cutoff radius of 12 Å was used for both short-range LJ and short-range electrostatic energies. Due to the inhomogeneity of the system, analytic corrections[56] were not used for the long-range contributions of the LJ interactions. Instead, the long-range LJ interactions as well as the long-range electrostatic interactions were computed using the particle−particle particle-mesh (PPPM) method.[59,65,66] The desired accuracies for the real-space and reciprocal parts of the long-range LJ interactions were set to 0.0001 and 0.002, respectively, while an accuracy of 10^{-6} was used for the long-range electrostatic energies. To test the adequacy of the PPPM accuracies for the LJ interactions, test simulations were performed for water and for each of the DESs in the pure form. Densities and RDFs were computed from these simulations and compared with those obtained from

https://doi.org/10.1021/acs.jpcb.1c07796
J. Phys. Chem. B 2021, 125, 12303−12314

simulations in which analytic tail corrections (and no PPPM calculations for LJ interactions) were used. Negligible differences were observed between the computed densities and RDFs of these simulations, thereby verifying the suitability of the selected PPPM accuracies.

To validate the force field parameters of Men−dec and Thy−dec, MD simulations were carried out for the computation of densities and shear viscosities of the neat DESs. For Men−dec, 100 menthol (50 L-menthol and 50 D-menthol) and 50 decanoic acid molecules were used, and for Thy−dec, 75 thymol and 75 decanoic acid molecules were used. The molar ratio of Thy−dec, at which the force field validation was performed (1:1), is different from the one used for Thy−dec/water simulations (1:2). Nevertheless, as observed from experiments,[55] the densities and shear viscosities of Thy−dec are not considerably affected by the liquid composition, that is, the densities and viscosities of Thy−dec are ca. 906 kg m^{-3} and 4.2 cP at the molar ratio of 1:1 and ca. 895 kg m^{-3} and 4.3 cP at the molar ratio of 1:2, respectively. The force field validation simulations consisted of an initial energy minimization (using the conjugate gradient method), followed by 50 ns of equilibration in the *NPT* ensemble, and 50 and 140 ns of equilibration and production in the *NVT* ensemble at the equilibrium densities, respectively. A pressure of 1 atm and temperatures of 343 and 328 K for Men−dec and Thy−dec, respectively, were used in the simulations. The average equilibrium box lengths were ca. 36 and 35.5 Å for Men−dec and Thy−dec, respectively. During the *NVT* production runs, the shear viscosities of the DESs were computed with the OCTP package[67] using a methodology described in our previous work.[46]

For the DES/water simulations, each phase (DES or water) was equilibrated separately. During the equilibration, the changes in the box dimensions were limited to only one direction, z (which would be perpendicular to the interface), while the box lengths in the other two dimensions were kept fixed at 42 Å for all systems. The simulation of each phase consisted of energy minimization and 20 ns (for water) or 30 ns (for DESs) of equilibration runs at 1 atm and 343 K in the *NPT* ensemble. For the DESs, before the *NPT* runs, the systems were annealed at 600 and 450 K (each for 5 ns) in the *NVT* ensemble to facilitate the equilibration. Two replicas of the equilibrated water phase were placed adjacent to the equilibrated DES phase, on the two opposite sides. Before this, the minimum image convention[56] was used to re-attach the fragments of molecules that were broken due the periodic boundary conditions in the z-direction (perpendicular to the interface) in the simulations of the pure phases.[32] The numbers of molecules and the HBA/HBD molar ratios used in the simulations of DES/water binary mixtures are listed in Table S19 of Supporting Information. The energy of each DES/water system was minimized to remove possible atomic overlaps at the interface. The DES/water mixture was subsequently equilibrated at various temperatures (323−363 K) and 1 atm for 55−95 ns (depending on the DES and temperature) in the *NPT* ensemble. The equilibrated box lengths of the TBAC−dec/water (with ca. 39 000 atoms), Thy−dec/water (with ca. 34 000 atoms), and Men−dec/water (with ca. 35 000 atoms) systems in the z-direction were typically around 225, 200, and 200 Å, respectively. Histograms of atomic positions in the z-direction were obtained during the runs using N_{bins} = 200 bins. The thickness of each bin was therefore $\delta z = L_z/N_{bins}$, where L_z is the simulation box length in the z-direction for each system. The number density profile of each molecule of type i in the z-direction was calculated as

$$\rho_i(z) = \frac{N_i(z)}{A_{xy}\delta z} \tag{1}$$

where $N_i(z)$ denotes the number of molecules of type i at position z and A_{xy} is the area of the xy side of the simulation box (parallel to the interface). For each molecule, the coordinates of a single representative atom were considered for the density profile calculations: the central nitrogen for the tetrabutylammonium cation and the hydroxyl oxygen atom for decanoic acid, thymol, and menthol. Note that the computed density profiles should be symmetric around half the box size in the z-direction. Deviations of this symmetry are indicative of sampling difficulties due to high viscosities.

The equilibration of each system was verified by monitoring the changes in the total energy, pressure, and the density profiles. After equilibration, *NVT* runs of 20−40 ns (depending on the DES and temperature) were carried out at temperatures of 323−363 K, during which the DES/water interfacial tensions and the water-in-DES solubilities (as well as the salt-in-water solubilities for TBAC−dec/water) were computed. Simulations at temperatures lower than 323 K were not considered due to the high viscosities of the systems. To improve the statistics for the computed interfacial tensions, five independent runs were used for the *NVT* simulation of each system (all runs starting from the same equilibrated configurations obtained from the *NPT* simulations), from which the averages and standard deviations were calculated. The DES/water interfacial tensions were computed according to[56,68]

$$\gamma = \frac{1}{2}L_z\left\langle P_{zz} - \frac{P_{xx} + P_{yy}}{2}\right\rangle \tag{2}$$

where the brackets $\langle\cdots\rangle$ denote an ensemble average; L_z is the box length in the z-direction (perpendicular to the interface); and P_{xx}, P_{yy}, and P_{zz} are the diagonal elements of the pressure tensor in the x, y, and z directions, respectively. The factor 1/2 accounts for the presence of two interfaces.

The mass fraction-based solubility of water in each DES (in units of wt %) was calculated using

$$s = \frac{m_{water}}{m_{water} + m_{DES}} \times 100\% \tag{3}$$

where m_{water} and m_{DES} are the total masses of water and DES present in the DES bulk phase, respectively, and the mass of the DES equals the sum of the masses of the HBA and HBD components. The total mass of each molecule type i (DES component or water) in the DES bulk phase was calculated by integrating its number density profile according to

$$m_i = \frac{M_i A_{xy}}{N_A}\int_{z_{max}}^{z_{min}} \rho_i(z)\, dz \tag{4}$$

where M_i is the molar mass of molecule type i, z is the position in the direction perpendicular to the interface, A_{xy} is the cross-section area of the simulation box parallel to the interface, N_A is the Avogadro number, and z_{max} and z_{min} are the maximum and minimum z-coordinates of the interface edges on the DES bulk phase side, respectively. The values of z_{min} and z_{max} were chosen based on the density profiles, and we verified that the calculated value of m_i did not depend on their precise values.

https://doi.org/10.1021/acs.jpcb.1c07796
J. Phys. Chem. B 2021, 125, 12303−12314

Table 1. Computed Densities and Shear Viscosities of Thy−dec (a Molar Ratio of 1:1) Using Different Charge Scaling Factors and Men−Dec (a Molar Ratio of 1:2), Compared with Experimental Data[54,55a]

DES	T/[K]	f_q	ρ^{sim}/[kg m^{-3}]	ρ^{exp}/[kg m^{-3}]	η^{sim}/[cP]	η^{exp}/[cP]
TBAC−dec[b]	323	0.6	884.2	901.0	75.8	68.3
Thy−dec	328	0.7/1	899.4	906.6	5.3	4.2
		0.8/0.8	894.7		4.5	
Men−dec	343	0.8/1	859.3	862.5	3.7	3.4

[a]The density and shear viscosity of TBAC−dec (molar ratio of 1:2), as computed in our previous work,[46] using a charge scaling factor of 0.6 have also been listed and compared with the experimental data by van Osch et al.[8] Error bars in computed densities are smaller than 1%. [b]Simulation results from our previous study.[46]

Similar calculations were performed to obtain the solubility of the HBA (salt) component of TBAC−dec in the aqueous phase.

The number densities of different types of hydrogen bonds, that is, the number of each hydrogen bond type divided by $A_{xy}\delta z$ (similar to eq 1), were calculated based on MD trajectories (100−200 snapshots from the last 20 ns of the production runs) as a function of the z-coordinate using an in-house code. A total of 200 bins were used to compute the histograms for the number densities of the hydrogen bonds. Following other simulation studies of DESs,[23,47] a donor-hydrogen-acceptor angle of 30° and a cutoff distance of 3.5 Å[23,47,69−71] were used as the criteria for the detection of hydrogen bonds.

3. RESULTS AND DISCUSSION

3.1. Force Field Validation. Different charge scaling values (0.6−0.9) were used in the computations of the interfacial properties of TBAC−dec with water. In our previous study,[46] a charge scaling factor of 0.6 yielded the best agreement of the computed transport properties and density of neat TBAC−dec with experimental data. Consistently, from test simulations in the present work, it was found that the shear viscosities of neat Thy−dec (a molar ratio of 1:1) and Men−dec (a molar ratio of 1:2) are significantly overestimated (by a factor of ca. 3.6 for both DESs) without the use of charge scaling, compared to experimental data.[54,55] Two sets of charge scaling factors were found to yield reasonably accurate densities and shear viscosities for Thy−dec: 0.7 for thymol and 1.0 for decanoic acid (denoted by "f_q = 0.7/1") and 0.8 for both thymol and decanoic acid (denoted by "f_q = 0.8/0.8"). To investigate the effect of charge scaling on the computed interfacial properties, both charge scaling sets were used for Thy−dec in the production runs of the Thy−dec/water simulations. For Men−dec, a charge scaling of 0.8 for menthol and a charge scaling of 1 for decanoic acid (denoted by "f_q = 0.8/1") resulted in accurate density and shear viscosity calculations. The results of the force field validation are presented in Table 1 for all the DESs and charge scaling sets and compared with available experimental data.[8,54,55]

3.2. Density Profiles and Interfacial Tensions. The number density profiles were computed for different components (i.e., molecule types) of the DESs using eq 2. The density profile results for TBAC−dec/water mixtures at 363 K with charge scaling factors of 0.6 and 0.8 are presented in Figures 1 and 2, respectively, accompanied by typical snapshots of the systems. The DES/water interfaces (indicated by blue shaded areas in Figures 1 and 2) were identified as regions where the densities of the mixture components change from the constant densities in the water phase to the constant densities in the DES phase. Based on this definition, the

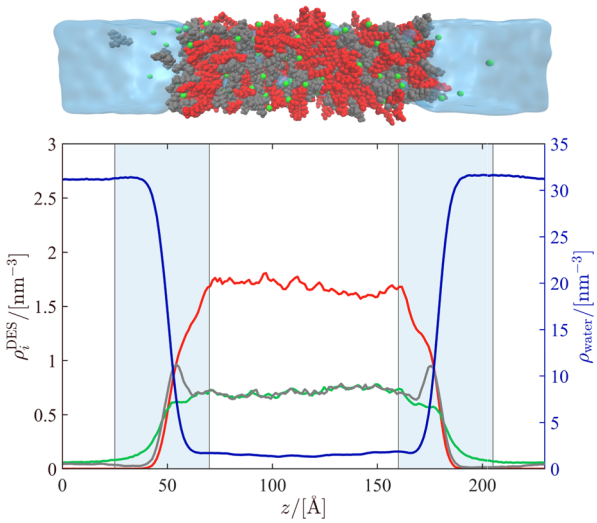

Figure 1. Computed number density profiles (number of molecules per nm^3) of DES components i (left vertical axis) and water (right vertical axis) in the TBAC−dec/water system at 363 K and 1 atm using a charge scaling factor of f_q = 0.6 for HBA. A typical snapshot of the same system is shown above the plot. The red, green, gray, and blue colors correspond to decanoic acid (HBD), chloride (anion), choline (cation), and water (shown in the snapshot using the blue surfaces), respectively. For the density profiles of decanoic acid and choline, the coordinates of the hydroxyl oxygen and the nitrogen atoms were used, respectively. The DES/water interfaces are indicated in the plot using blue shaded areas.

thickness of each interface was estimated from the difference in the z-coordinates of the two interface edges. It can be observed from Figure 1 that with f_q = 0.6, the structure of TBAC−dec (at the center) remains mostly intact, with very small amounts of cations and anions transferred to the aqueous phase (on the two opposite sides of the DES). This is in sharp contrast to experimental observations where it has been shown that considerable amounts of the HBA (i.e., the salt composed of the cation and anion) of TBAC−dec leach to the water phase.[8,16,18] For instance, van Osch et al.[8] found a 34.8% leaching of the salt (i.e., the mass of the leached salt divided by the total mass of the salt in the DES) into water at 298 K, indicating a salt-in-water solubility of ca. 13.5 wt %. As can be observed in Figure 1, the cation density profile shows a peak at the intersection of the water and decanoic acid profiles, indicating a favorable position for the cation that allows for interactions with both the water and decanoic acid. Figure 2 shows the density profiles of the TBAC−dec/water system using a charge scaling factor of 0.8 for the salt. It can be observed that with f_q = 0.8, a significant leaching of the salt into water occurs, which changes the structure and composition of the neat DES, and results in similar densities of the cation and

https://doi.org/10.1021/acs.jpcb.1c07796
J. Phys. Chem. B 2021, 125, 12303−12314

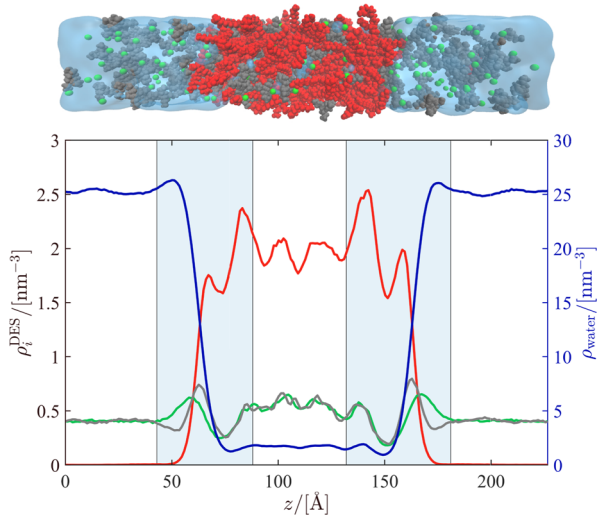

Figure 2. Computed number density profiles (number of molecules per nm^3) of DES components i (left vertical axis) and water (right vertical axis) in the TBAC−dec/water system at 363 K and 1 atm using a charge scaling factor of $f_q = 0.8$ for HBA. A typical snapshot of the same system is shown above the plot. The red, green, gray, and blue colors correspond to decanoic acid (HBD), chloride (anion), choline (cation), and water (shown in the snapshot using the blue surfaces), respectively. For the density profiles of decanoic acid and choline, the coordinates of the hydroxyl oxygen and the nitrogen atoms were used, respectively. The DES/water interfaces are indicated in the plot using blue shaded areas.

anion in water, compared to those in the DES bulk phase. This is due to the stronger electrostatic interactions of the cation and anion with water at $f_q = 0.8$, compared to $f_q = 0.6$. Consistently, Paul et al.[41] showed, using MD simulations of TBAC−dec/water with the charge scaling factor of $f_q = 1$ (no scaling), a complete leaching of the salt into water. As shown in Figure 2, both the cation and anion show peaks at the intersections of the water and decanoic acid density profiles, possibly due to the simultaneously maximized HBD−HBA and HBA−water interactions. Although comparable interface thicknesses are obtained using charge scaling factors of 0.6 and 0.8 (ca. 45 Å) at $f_q = 0.8$, due to the leaching of HBA, the thickness of the DES bulk phase is smaller, while the thickness of the aqueous phase is larger. Using both charge scaling factors, decanoic acid and water are immiscible, in agreement with experimental observations.[8,16,18]

The density profiles of the TBAC−dec/water system at 343 K using different charge scaling factors (0.6−0.9) are presented in Figure S6 of Supporting Information. Similar to the results shown in Figures 1 and 2, an increase in the charge scaling factor increases the leaching of the salt into water at 343 K (Figure S6). Interestingly, comparable density profiles are obtained using the charge scaling factors of 0.8 and 0.9, which implies an upper threshold for the amount of leaching of the salt into water. By comparing Figure S6 with Figures 1 and 2, it can be deduced that the density profiles and thus the hydrophobicity of TBAC−dec are not considerably affected by temperature. Using eqs 3 and 4, the solubility of the salt (HBA) component of TBAC−dec in water at 363 K (the average solubilities of the cation and anion), with the charge scaling factor of 0.6, is computed as 2.4 wt %, which is significantly underestimated compared to the experimental value of 13.5 wt % at 298 K. Therefore, while the properties of neat TBAC−dec are accurately reproduced with $f_q = 0.6$,[46] the computed salt-in-water solubility is much lower than the experimental value (assuming a negligible effect of temperature on the solubility). Using $f_q = 0.8$, the salt-in-water solubility of TBAC−dec at 363 K is computed as 19.9 wt %, which is in a better agreement with the experimental value. The water-in-DES solubilities for TBAC−dec at 363 K using charge scaling factors of 0.6 and 0.8 are computed as 5.0 and 4.8 wt %, respectively, which are both in reasonable agreement with the experimental value of 6.9 wt % at 298 K.[8]

From the results of Figures 1 and 2 (and Figure S6), it is indicated that the charge scaling factor of 0.8 for TBAC−dec is better suited for the computation of the properties of the DES/water biphasic system, compared to the charge scaling factor of 0.6. In our previous study,[46] it was shown that using charge scaling factors larger than 0.6, while not considerably affecting the density, led to highly overestimated shear viscosities of TBAC−dec (unless the LJ interactions from the GAFF force field were also scaled). For instance, the shear viscosities of TBAC−dec at 353 K using charge scaling factors of 0.6 and 0.7 were computed as 51.0 and 19.4 cP, respectively, whereas the (extrapolated) experimental viscosity at this temperature is 16.8 cP. The shear viscosity of TBAC−dec with $f_q = 0.8$ could not be computed in that study due to non-converging mean squared displacements, which is indicative of very high viscosities. Such a high viscosity is also reflected in the relatively large fluctuations of the densities of the DES components (particularly HBD) in Figure 2, suggesting a hindered motion of the molecules and thus a more difficult density sampling. This increase in the density fluctuations with an increase in the charge scaling factor is more accentuated at 343 K (Figure S6 in Supporting Information) due to higher viscosities. Therefore, large charge scaling values, which may be appropriate for DES/water interface computations, are not suitable for computing the properties of neat DESs. It is important to note that in the study by Paul et al.,[41] where $f_q = 1$ was used, the authors did not compute the properties of neat DESs (only DES/water properties were computed), except for a few densities, which may reduce the transferability of their force fields for such computations.

The computed density profiles for the components of the Thy−dec/water mixture at 363 K using $f_q = 0.7/1$ and a typical snapshot of the system are presented in Figure 3. It can be observed that Thy−dec is almost completely immiscible with water, with a computed water-in-DES solubility of 0.71 wt %, consistent with experiments for Thy−dec with a molar ratio of 1:1 at 298 K.[72] The density profiles for Thy−dec/water with charge scaling factors of $f_q = 0.8/0.8$ are shown in Figure S7 of Supporting Information. By comparing Figures 3 and S7, it is found that the density profiles of the various components are nearly identical between the two charge scaling sets. For both charge scaling sets, the thickness of each DES/water interface is ca. 35 Å. Using the charge scaling factors of $f_q = 0.8/0.8$, the water-in-DES solubility for the Thy−dec/water system is computed as 0.92 wt %, which is comparable to that obtained with $f_q = 0.7/1$. In Figures 3 and S7, two large peaks can be observed for the (hydroxyl oxygen of) decanoic acid at each interface, followed by minimums. As shown in Figure S8 of Supporting Information, these minimums correspond to density profile peaks for the terminal carbon of decanoic acid (on the opposite side of the molecule with respect to the oxygen atom). Therefore, the density profile peaks of decanoic acid in Figures 3 and S7 are possibly caused by the fact that the

https://doi.org/10.1021/acs.jpcb.1c07796
J. Phys. Chem. B 2021, 125, 12303−12314

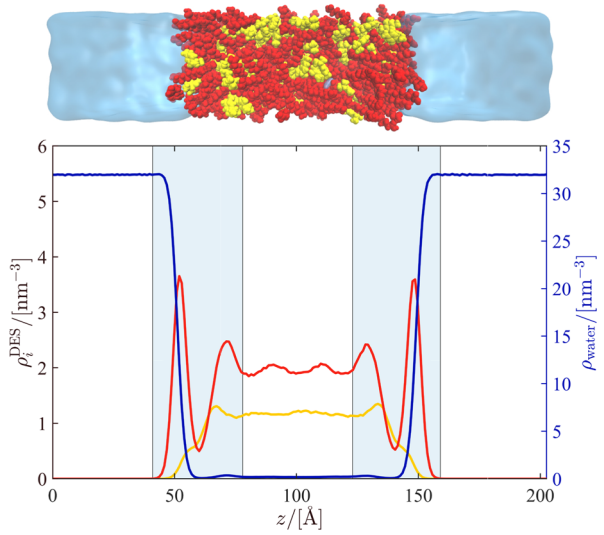

Figure 3. Computed number density profiles (number of molecules per nm^3) of DES components i (left vertical axis) and water (right vertical axis) in the Thy−dec/water mixture at 363 K and 1 atm using the charge scaling factors f_q = 0.7/1. A typical snapshot of the same system is shown above the plot. The red, yellow, and blue colors correspond to decanoic acid (HBD), thymol (HBA), and water (shown in the snapshot using the blue surfaces), respectively. For the density profiles of decanoic acid and thymol, the coordinates of the hydroxyl oxygen atoms were used. The DES/water interfaces are indicated in the plot using blue shaded areas.

decanoic acid molecules are aligned such that their hydroxyl or carbonyl oxygen atoms can form hydrogen bonds with the water molecules at the interface (i.e., with the oxygen and terminal carbon atoms of decanoic acid toward the water and DES phases, respectively). This hypothesis is supported by a close-up snapshot of the Thy−dec/water system, presented in Figure 4, which shows the orientation of decanoic acid molecules at the interface. The density profiles of the Thy−dec/water components at 343 K are presented in Figure S9 of

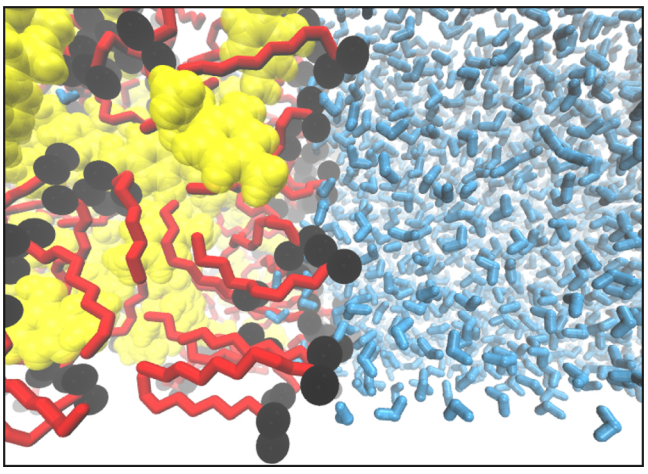

Figure 4. Close-up snapshot of the Thy−dec/water interface at 363 K and 1 atm, with the charge scaling factors of f_q = 0.7/1, showing the alignment of the oxygen atoms (black van der Waals surfaces) of decanoic acid toward the aqueous phase. The carbon atoms of decanoic acid are colored red (the hydrogen atoms are omitted in the snapshot for clarity). The yellow and blue molecules are thymol and water, respectively.

Supporting Information for both charge scaling sets. It can be observed that similar to TBAC−dec/water, the effect of temperature on the density profiles of Thy−dec/water and the hydrophobicity of Thy−dec is very small.

The computed density profiles of the Men−dec/water components at 363 K and a typical system snapshot are shown in Figure 5. Similar to the Thy−dec/water density profiles

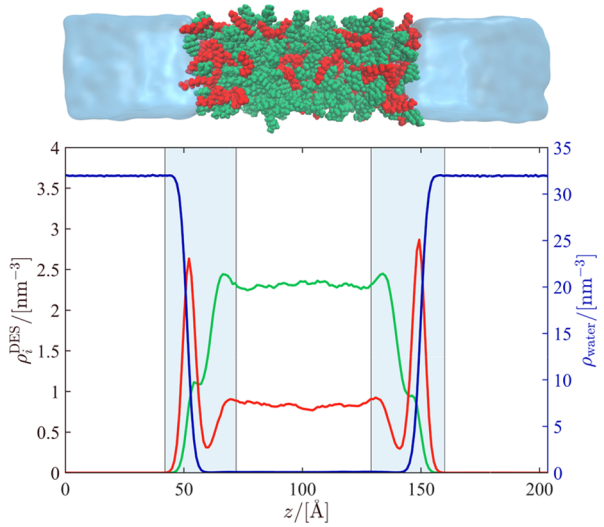

Figure 5. Computed number density profiles (number of molecules per nm^3) of DES components i (left vertical axis) and water (right vertical axis) in the Men−dec/water mixture at 363 K and 1 atm using the charge scaling factors of f_q = 0.8/1. A typical snapshot of the same system is shown above the plot. The red, green, and blue colors correspond to decanoic acid (HBD), menthol (HBA), and water (shown in the snapshot using the blue surfaces), respectively. For the density profiles of decanoic acid and menthol, the coordinates of the hydroxyl oxygen atoms were used. The density profile of menthol in the plot and its representation in the snapshot include both D-menthol and L-menthol molecules. The DES/water interfaces are indicated in the plot using blue shaded areas.

(Figure 3), the density profiles of Men−dec/water indicate a nearly complete immiscibility of the DES with water. The water-in-DES solubility was computed as 0.4 wt %, which compared to the experimental value of 2.1 wt % at 295 K[73] indicates an underestimation of the solubility of water in Men−dec from the simulations (assuming a negligible effect of temperature on the solubility). The interface thickness of the simulated Men−dec/water system is roughly 30 Å. The density profiles for Men−dec/water show very similar features to the ones observed for Thy−dec/water, that is, the large peaks of the decanoic acid profile (due to the alignment of decanoic acid molecules to form hydrogen bonds with water), and a two-step increase in the density of HBA (menthol or thymol) from the aqueous phase to the DES phase. The relative values of the HBD and HBA densities in the DES phase of Men−dec/water are nevertheless different from those in Thy−dec/water due to the different HBA/HBD molar ratios of the two DESs. The density profiles of the Men−dec/water components at 343 K are presented in Figure S10 of Supporting Information, which in comparison to the density profiles in Figure 5 indicate a negligible influence of temperature on the DES/water interface and the hydrophobicity of Men−dec. It is important to note that in the simulations of Men−dec/water, the HBA component of Men−dec consisted of equal amounts

https://doi.org/10.1021/acs.jpcb.1c07796
J. Phys. Chem. B 2021, 125, 12303−12314

of D-menthol and L-menthol (racemic mixture). However, negligible differences were observed for the density profiles and hydrogen bonds (the following section) between D-menthol and L-menthol. Therefore, the density profiles and hydrogen bonds of D-menthol and L-menthol were lumped together as a single "menthol" component, which is used throughout the article. Since decanoic acid is more hydrophilic than menthol (following from density profiles), having more menthol compared to decanoic acid (a molar ratio of 2:1) may lead to a larger interfacial tension and hydrophobicity compared to having less menthol (e.g., 1:2 as used for the other DESs).

The interfacial tensions of the DESs with water were computed from *NVT* simulations at different temperatures using eq 2. The results, presented in Figure 6, indicate that the

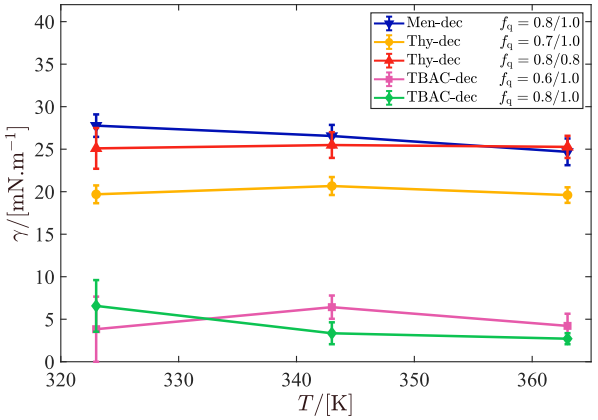

Figure 6. Computed DES/water interfacial tensions for the various DESs and charge scaling sets as a function of temperature (at 1 atm). The lines are drawn to guide the eye.

DES/water interfacial tensions of all the DESs at all charge scaling factors are independent of temperature (within the error bars). This further verifies that the hydrophobicity of the studied DESs is insensitive to temperature. As shown in Figure 6, TBAC−dec has the smallest interfacial tension with water and thus the lowest hydrophobicity. The differences between the TBAC−dec/water interfacial tensions at f_q = 0.6 and f_q = 0.8 generally fall within the error bars (i.e., the standard deviation of the interfacial tensions from the five independent runs) shown in Figure 5, although from the density profiles and simulation snapshots (Figures 1 and 2), it can be concluded that f_q = 0.6 leads to a higher hydrophobicity for TBAC−dec. The high DES/water interfacial tensions of Thy−dec and Men−dec corroborate the large extent of the hydrophobicity of these DESs, deduced from the density profiles and simulation snapshots (Figures 3 and 5). Unlike for TBAC−dec, the DES/water interfacial tension of Thy−dec highly depends on the charge scaling set used in the simulations, that is, the scaling factors f_q = 0.8/0.8 result in a larger interfacial tension, compared to f_q = 0.7/1. This implies the pivotal role of decanoic acid in lowering the interfacial energy of Thy−dec with water through electrostatic forces (possibly hydrogen bonds). Considering the charge scaling factors f_q = 0.7/1 for Thy−dec, the relative magnitudes of the computed interfacial tensions with water (and thus the hydrophobicity) of the DESs are in the following order: TBAC−dec < Thy−dec < Men−dec. Consistently, this is the reverse of the order of water-in-DES solubilities, calculated from the density profiles, which is in agreement with the order of water-in-DES solubilities described by Florindo et al.,[7] based on the DES constituents (menthol < thymol < quaternary ammonium salts).

3.3. Hydrogen Bond Analysis. The number densities of various types of hydrogen bonds (ρ_{Hb}) were calculated as a function of the z-coordinate (perpendicular to the interface) for all the DESs and charge scaling sets. The hydrogen bond analysis results are presented in Figures 7−9 for TBAC−dec/

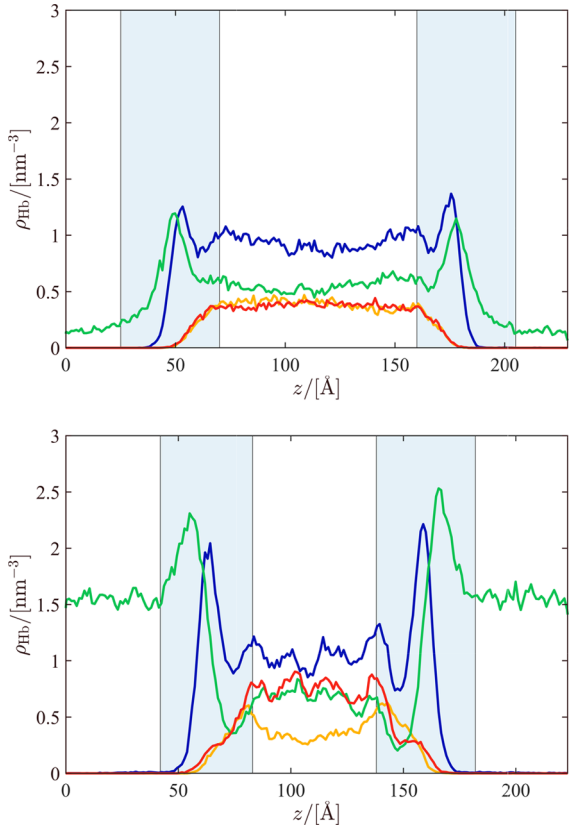

Figure 7. Computed hydrogen bond number densities (number of hydrogen bonds per nm^3) for the TBAC−dec/water system at 363 K and 1 atm, with charge scaling factors of (a) f_q = 0.6, and (b) f_q = 0.8. The blue, green, yellow, and red colors correspond to water−decanoic acid, water−chloride, decanoic acid−decanoic acid, and chloride−decanoic acid hydrogen bonds, respectively. The blue shaded areas indicate the interfaces, as deduced from the density profiles in Figures 1 and 2.

water, Thy−dec/water, and Men−dec/water binary mixtures, respectively. The DES/water interfaces, as deduced from the density profiles in Figures 1−3,5, are also shown in Figures 7−9 using blue shaded areas. As can be observed in Figure 7, for TBAC−dec/water (at 363 K), at both charge scaling factors, the chloride anion forms hydrogen bonds with water in the aqueous phase, with f_q = 0.8 resulting in a larger number of chloride−water hydrogen bonds, compared to f_q = 0.6. Using the scaling factor f_q = 0.6, the total number of hydrogen bonds of chloride (i.e., the sum of the number of chloride−decanoic acid and chloride−water hydrogen bonds) in the DES phase is larger than that in the aqueous phase (Figure 7a). This is in sharp contrast to the results for f_q = 0.8 (Figure 7b), where the total number of hydrogen bonds of chloride in the DES phase is comparable to the number of chloride−water hydrogen bonds in the aqueous phase. This may explain the observed leaching of chloride into water and the more or less constant

https://doi.org/10.1021/acs.jpcb.1c07796
J. Phys. Chem. B 2021, 125, 12303−12314

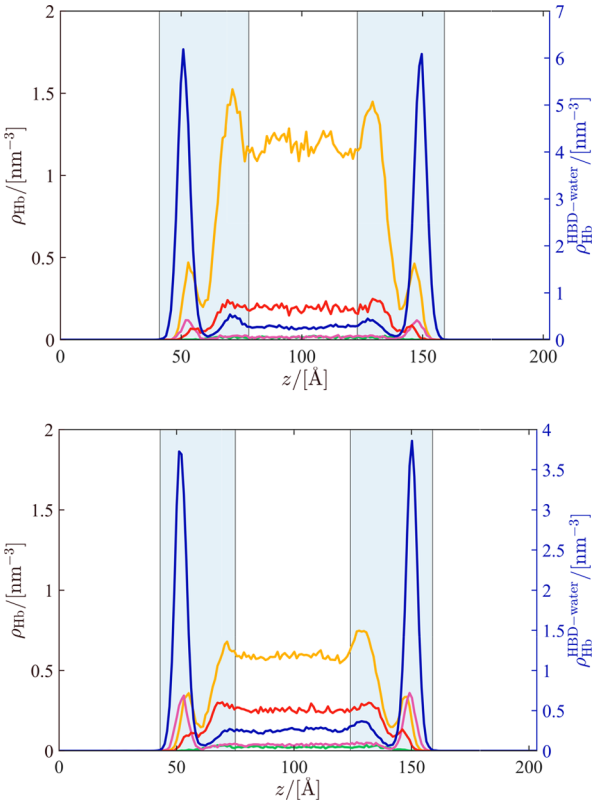

Figure 8. Computed hydrogen bond number densities (number of hydrogen bonds per nm^3) for the Thy−dec/water system at 363 K and 1 atm, with charge scaling factors of (a) f_q = 0.7/1, and (b) f_q = 0.8/0.8. The blue, green, yellow, red, and pink colors correspond to water−decanoic acid (right vertical axis), thymol−thymol, decanoic acid−decanoic acid, thymol−decanoic acid, and water−thymol hydrogen bonds, respectively. The blue shaded areas indicate the interfaces, as deduced from the density profiles in Figures 3 and S7.

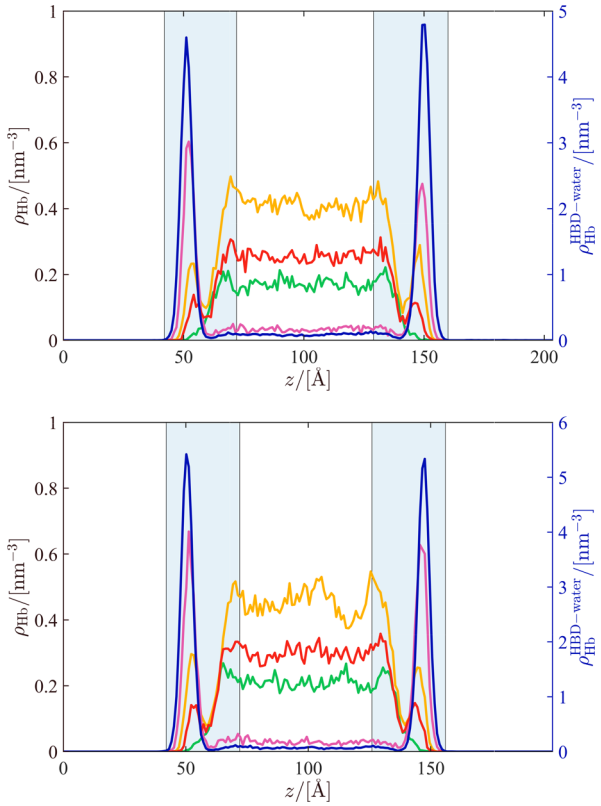

Figure 9. Computed hydrogen bond number densities (number of hydrogen bonds per nm^3) for the Men−dec/water system, with charge scaling factors of f_q = 0.8/1, at 1 atm and (a) 343 and (b) 363 K. The blue, green, yellow, red, and pink colors correspond to water−decanoic acid (right vertical axis), menthol−menthol, decanoic acid−decanoic acid, menthol−decanoic acid, and water−menthol hydrogen bonds, respectively. The blue shaded areas indicate the interfaces, as deduced from the density profiles in Figures 5 and S10.

number density of chloride throughout the whole simulation box (Figure 2). The leaching of the cation into water, particularly at f_q = 0.8, likely occurs as a result of the electrostatic interactions of the cation with water and with the leached chloride. These findings on the leaching of ions are consistent with the MD simulation results by Paul et al.,[41] where a large number of hydrogen bonds were formed between the chloride anion of TBAC−octanoic acid (a molar ratio of 1:1 and f_q = 1) and water, substantially contributing to the leaching of the salt into the aqueous phase.

It can be observed in Figure 7 that at f_q = 0.6, the number of decanoic acid−decanoic acid hydrogen bonds in the DES phase is similar to that of chloride−decanoic acid hydrogen bonds, whereas with a larger anion charge (f_q = 0.8), the number of chloride−decanoic acid hydrogen bonds is larger than that of the decanoic acid−decanoic acid hydrogen bonds. The water molecules form a considerable number of hydrogen bonds with both the anion and decanoic acid in the DES phase, driving the dissolution of water into the DES. Large peaks are observed at each interface for decanoic acid−water hydrogen bonds. The presence of these peaks supports the hypothesis that decanoic acid molecules align their acidic ends toward the water phase (as shown in Figures 4 and S8 for Thy−dec/water) to maximize the hydrogen bonds with water molecules. While decanoic acid−decanoic acid, decanoic acid−chloride, and decanoic acid−water hydrogen bond interactions compete more equally in the DES bulk phase, at the interface, the hydrogen bond interactions of decanoic acid are dominated by those with the water molecules. With an increase in the charge scaling factor from 0.6 to 0.8, the intensity of the decanoic acid−water hydrogen bond peaks increases, possibly due to a stronger alignment of decanoic acid oxygen atoms toward the aqueous phase, which may be caused by the leaching of the anion into water. The number densities of decanoic acid−decanoic acid and decanoic acid−water hydrogen bonds at f_q = 0.8 were decomposed based on the functional group of decanoic acid participating in the hydrogen bonds, that is, carbonyl or hydroxyl, and the results are presented in Figure S11 of Supporting Information. It can be observed in Figure S11 that decanoic acid−decanoic acid hydrogen bonds mainly occur between the carbonyl and hydroxyl groups, with negligible hydroxyl−hydroxyl hydrogen bonds (consistent with our previous MD study of neat TBAC−dec[46]). For decanoic acid−water hydrogen bonds, significant contributions are observed from both the hydroxyl and carbonyl groups of decanoic acid (a larger contribution by the hydroxyl groups). The hydrogen bond number densities of TBAC−dec/water at 343 K are presented in Figure S12 of Supporting Information. No significant difference is found in the hydrogen bond networks of TBAC−dec/water between the two temperatures (for both charge scaling factors), which is consistent with the observations from the computed density profiles.

https://doi.org/10.1021/acs.jpcb.1c07796
J. Phys. Chem. B 2021, 125, 12303−12314

The hydrogen bond number densities of Thy−dec/water at 363 K are presented in Figure 8 for the charge scaling sets f_q = 0.7/1 and f_q = 0.8/0.8. It can be observed that using both charge scaling sets, large peaks occur for water−decanoic acid hydrogen bonds at the interface, which may be caused by the larger number of water molecules present at the interface compared to the DES bulk phase and possibly also the alignment of the oxygen atoms of decanoic acid toward the aqueous phase (Figure 4). This explains the large peaks of the density profile of decanoic acid in Figures 3 and S7. It can be observed that the numbers of decanoic acid−water and decanoic acid−decanoic acid hydrogen bonds are significantly larger for f_q = 0.7/1 (with peak heights of ca. 6.1 and 1.5 nm^{-3}, respectively), compared to f_q = 0.8/0.8 (with peak heights of 3.8 and 0.7 nm^{-3}, respectively), due the larger partial atomic charges of decanoic acid at f_q = 0.7/1. The larger number of decanoic acid−water hydrogen bonds for f_q = 0.7/1 is likely responsible for the lower Thy−dec/water interfacial tensions at f_q = 0.7/1, compared to f_q = 0.8/0.8 (Figure 6). The thymol−water hydrogen bond densities show small peaks at the interfaces due to the interactions of the hydroxyl group of thymol with water, whereas a negligible number of thymol−water hydrogen bonds occur within the DES phase. A very small number of thymol−thymol hydrogen bonds is formed in the DES bulk phase, while a more considerable number of thymol molecules participate in hydrogen bonding with decanoic acid. The hydrogen bond number densities for Thy−dec/water at 343 K are provided in Figure S13 of Supporting Information, showing an insignificant effect of temperature on the hydrogen bond network of the system (compared to Figure 8).

For Men−dec/water, the hydrogen bond number densities of the various components are shown in Figure 9 for temperatures of 343 and 363 K. It can be observed that similar to TBAC−dec/water and Thy−dec/water mixtures, the effect of temperature on all hydrogen bond densities in Men−dec/water is negligible. As shown in Figure 9, large peaks are observed at the interfaces for the water−decanoic acid hydrogen bond densities, while comparatively smaller peaks are found for the densities of menthol−water, menthol−decanoic acid, and decanoic acid−decanoic acid hydrogen bonds. The menthol−decanoic acid and decanoic acid−decanoic acid hydrogen bonds mostly occur in the DES bulk phase. Similar to TBAC−dec/water and Thy−dec/water, the large number density peaks of the water−decanoic acid hydrogen bonds at the interfaces of Men−dec/water may be due to the higher concentration of water at the interfaces compared to the DES bulk phase and the alignment of decanoic acid oxygen atoms toward the aqueous phase. The total numbers of water−menthol and water−decanoic acid hydrogen bonds in the Men−dec/water mixture at 363 K were calculated as ca. 16 and 113, respectively. This is in agreement with the MD simulation results of Paul et al.,[41] where for a mixture of Men−dec (with a molar ratio of 1:1 and no charge scaling) and water, a significantly larger number of water−decanoic acid hydrogen bonds were found, compared to that of water−menthol hydrogen bonds. The large number of water−decanoic acid hydrogen bonds at the interfaces, as observed in Figure 9, justifies the large density profile peaks for (the hydroxyl oxygen of) decanoic acid, in Figure 5. In contrast to the Thy−dec/water system, in Men−dec/water, the number of HBA−HBA (menthol−menthol) hydrogen bonds in the DES bulk phase is comparable to the numbers of the other hydrogen bonds (i.e., menthol−decanoic acid and decanoic acid−decanoic acid hydrogen bonds), which may mostly be due the larger mole fraction of menthol in Men−dec, compared to that of thymol in Thy−dec.

From the study of the density profiles and the hydrogen bond analysis, it can be concluded that the hydrogen bonding between the various components, particularly the decanoic acid−water and anion−water (in TBAC−dec) hydrogen bonds, plays a crucial role in the phase behavior and interfacial properties of DESs in the presence of water. The effect of charge scaling was found to have a crucial influence on the DES/water interface of TBAC−dec and the leaching of the salt into the aqueous phase. For Thy−dec, using a charge scaling set with larger partial charges for decanoic acid (f_q = 0.7/1) resulted in a larger number of decanoic acid−water hydrogen bonds. Although this did not have a considerable effect on the density profiles, it led to lower Thy−dec/water interfacial tensions. This means that for an accurate prediction of the DES/water interface, a complete set of relevant parameters, for example, density profiles, interfacial tension, and hydrogen bond densities, must be computed. For future research, it would be beneficial to consider a wider range of HBA and HBD components and HBA/HBD mixing ratios for the computation of the DES/water interfacial properties. This will be crucial to achieve a more systematic understanding of the effect of the chemical structures of the DES constituents and the DES liquid composition on these properties.

4. CONCLUSIONS

The interfacial properties of binary mixtures of hydrophobic DESs and water were computed for TBAC−dec (1:2), Thy−dec (1:2), and Men−dec (2:1) DESs. The GAFF force field was used for all DESs, and the SPC/E model was used for water. Different charge scaling factors were considered for TBAC−dec (f_q = 0.6−0.9) and Thy−dec (f_q = 0.7/1 and f_q = 0.8/0.8). The density profiles of the various components of the mixtures were computed from MD trajectories as a function of the z-direction (perpendicular to the interface). The water-in-DES solubilities (and salt-in-water solubilities for TBAC−dec) were computed from the density profiles. Based on snapshots of atomic coordinates, the number densities of various types of hydrogen bonds were calculated. The interfacial tensions of the DES/water systems were computed at various temperatures. It was observed that the interfacial tensions of the DES/water mixtures and thus the hydrophobicity of the DESs were not considerably influenced by temperature. Using the charge scaling factors f_q = 0.7/1 for Thy−dec, the hydrophobicity of the DESs was computed as TBAC−dec < Thy−dec < Men−dec, consistent with the experimental observations. The density profiles of all DES/water mixtures showed significant peaks for (the hydroxyl oxygen atom of) decanoic acid, partly associated with an alignment of the oxygen atoms of decanoic acid molecules toward the aqueous phase for maximized hydrogen bond interactions with water. This was corroborated by the hydrogen bond number densities and a close-up visualization of the Thy−dec/water interface. While using f_q = 0.6 for TBAC−dec resulted in a small amount of leaching of the salt into water and thus an underestimated salt-in-water solubility, the charge scaling factor f_q = 0.8 resulted in a considerable leaching of the salt and a salt-in-water solubility that was in better agreement with the experimental value. The number of hydrogen bonds between chloride and water in the TBAC−dec/water mixture was found to significantly increase

https://doi.org/10.1021/acs.jpcb.1c07796
J. Phys. Chem. B 2021, 125, 12303−12314

with an increase in the charge scaling factor, thereby contributing to the leaching of the anion (and thus the salt as a whole) into water. For Thy−dec and Men−dec, no leaching of the DES components into water was observed, and these DESs showed strongly hydrophobic behaviors and negligible water-in-DES solubilities. For the Thy−dec/water system, the use of different charge scaling sets for Thy−dec showed a negligible effect on the density profiles, while resulting in different interfacial tensions, due to different numbers of decanoic acid−water hydrogen bonds formed at the interfaces. The numbers of thymol−thymol and water−thymol interactions in the Thy−dec bulk phase were much smaller than those of other hydrogen bond types (e.g., thymol−decanoic acid hydrogen bonds). Small numbers of menthol−menthol, decanoic acid−decanoic acid, and menthol−decanoic acid hydrogen bonds were formed in the DES bulk phase of Men−dec/water. At the interfaces of Men−dec/water, a much larger number of decanoic acid−water hydrogen bonds was found, compared to the numbers of other hydrogen bond types (e.g., menthol−water hydrogen bonds). An interesting extension of our work would be to investigate how the interfacial properties of the individual components (HBD, HBA) differ from the interfacial properties of the DES.

■ ASSOCIATED CONTENT

Supporting Information

The Supporting Information is available free of charge at https://pubs.acs.org/doi/10.1021/acs.jpcb.1c07796.

Molecular structures and force field parameters (PDF)

■ AUTHOR INFORMATION

Corresponding Author

Thijs J. H. Vlugt − *Engineering Thermodynamics, Process & Energy Department, Faculty of Mechanical, Maritime and Materials Engineering, Delft University of Technology, 2628CB Delft, The Netherlands;* orcid.org/0000-0003-3059-8712; Email: t.j.h.vlugt@tudelft.nl

Authors

Hirad S. Salehi − *Engineering Thermodynamics, Process & Energy Department, Faculty of Mechanical, Maritime and Materials Engineering, Delft University of Technology, 2628CB Delft, The Netherlands*

Othonas A. Moultos − *Engineering Thermodynamics, Process & Energy Department, Faculty of Mechanical, Maritime and Materials Engineering, Delft University of Technology, 2628CB Delft, The Netherlands;* orcid.org/0000-0001-7477-9684

Complete contact information is available at: https://pubs.acs.org/10.1021/acs.jpcb.1c07796

Notes

The authors declare no competing financial interest.

■ ACKNOWLEDGMENTS

This work was sponsored by NWO Domain Science for the use of supercomputer facilities. T.J.H.V. acknowledges NWO-CW (Chemical Sciences) for a VICI grant.

■ REFERENCES

(1) Hansen, B. B.; Spittle, S.; Chen, B.; Poe, D.; Zhang, Y.; Klein, J. M.; Horton, A.; Adhikari, L.; Zelovich, T.; Doherty, B. W.; Gurkan, B.; Maginn, E. J.; Ragauskas, A.; Dadmun, M.; Zawodzinski, T. A.; Baker, G. A.; Tuckerman, M. E.; Savinell, R. F.; Sangoro, J. R. Deep Eutectic Solvents: A Review of Fundamentals and Applications. *Chem. Rev.* **2021**, *121*, 1232−1285.

(2) Zhang, Q.; De Oliveira Vigier, K.; Royer, S.; Jérôme, F. Deep Eutectic Solvents: Syntheses, Properties and Applications. *Chem. Soc. Rev.* **2012**, *41*, 7108−7146.

(3) Smith, E. L.; Abbott, A. P.; Ryder, K. S. Deep Eutectic Solvents (DESs) and Their Applications. *Chem. Rev.* **2014**, *114*, 11060−11082.

(4) Sarmad, S.; Xie, Y.; Mikkola, J. P.; Ji, X. Screening of Deep Eutectic Solvents (DESs) as Green CO_2 Sorbents: From Solubility to Viscosity. *New J. Chem.* **2017**, *41*, 290−301.

(5) van Osch, D. J. G. P.; Dietz, C. H. J. T.; Warrag, S. E. E.; Kroon, M. C. The Curious Case of Hydrophobic Deep Eutectic Solvents: A Story on the Discovery, Design, and Applications. *ACS Sustain. Chem. Eng.* **2020**, *8*, 10591−10612.

(6) Marcus, Y. *Deep Eutectic Solvents*; Springer International Publishing: Cham, Switzerland, 2019; Vol. *1*.

(7) Florindo, C.; Branco, L. C.; Marrucho, I. M. Quest for Green-Solvent Design: From Hydrophilic to Hydrophobic (Deep) Eutectic Solvents. *ChemSusChem* **2019**, *12*, 1549−1559.

(8) van Osch, D. J. G. P.; Zubeir, L. F.; van den Bruinhorst, A.; Rocha, M. A. A.; Kroon, M. C. Hydrophobic Deep Eutectic Solvents as Water-immiscible Extractants. *Green Chem.* **2015**, *17*, 4518−4521.

(9) Zubeir, L. F.; van Osch, D. J. G. P.; Rocha, M. A. A.; Banat, F.; Kroon, M. C. Carbon Dioxide Solubilities in Decanoic Acid-based Hydrophobic Deep Eutectic Solvents. *J. Chem. Eng. Data* **2018**, *63*, 913−919.

(10) Dietz, C. H. J. T.; van Osch, D. J. G. P.; Kroon, M. C.; Sadowski, G.; van Sint Annaland, M.; Gallucci, F.; Zubeir, L. F.; Held, C. PC-SAFT Modeling of CO_2 Solubilities in Hydrophobic Deep Eutectic Solvents. *Fluid Phase Equilib.* **2017**, *448*, 94−98.

(11) Haider, M. B.; Jha, D.; Kumar, R.; Marriyappan Sivagnanam, B. Ternary Hydrophobic Deep Eutectic Solvents for Carbon Dioxide Absorption. *Int. J. Greenhouse Gas Control* **2020**, *92*, 102839.

(12) Cao, J.; Yang, M.; Cao, F.; Wang, J.; Su, E. Tailor-made Hydrophobic Deep Eutectic Solvents for Cleaner Extraction of Polyprenyl Acetates from *Ginkgo biloba* Leaves. *J. Clean. Prod.* **2017**, *152*, 399−405.

(13) Cao, J.; Yang, M.; Cao, F.; Wang, J.; Su, E. Well-designed Hydrophobic Deep Eutectic Solvents as Green and Efficient Media for the Extraction of Artemisinin from *Artemisia annua* Leaves. *ACS Sustain. Chem. Eng.* **2017**, *5*, 3270−3278.

(14) Tereshatov, E. E.; Boltoeva, M. Y.; Folden, C. M. First Evidence of Metal Transfer into Hydrophobic Deep Eutectic and Low-Transition-Temperature Mixtures: Indium Extraction from Hydrochloric and Oxalic Acids. *Green Chem.* **2016**, *18*, 4616−4622.

(15) Phelps, T. E.; Bhawawet, N.; Jurisson, S. S.; Baker, G. A. Efficient and Selective Extraction of $^{99mm}TcO^{-4}$ from Aqueous Media Using Hydrophobic Deep Eutectic Solvents. *ACS Sustain. Chem. Eng.* **2018**, *6*, 13656−13661.

(16) Ruggeri, S.; Poletti, F.; Zanardi, C.; Pigani, L.; Zanfrognini, B.; Corsi, E.; Dossi, N.; Salomäki, M.; Kivelä, H.; Lukkari, J.; Terzi, F. Chemical and Electrochemical Properties of a Hydrophobic Deep Eutectic Solvent. *Electrochim. Acta* **2019**, *295*, 124−129.

(17) Tang, W.; Dai, Y.; Row, K. H. Evaluation of Fatty Acid/Alcohol-based Hydrophobic Deep Eutectic Solvents as Media for Extracting Antibiotics from Environmental Water. *Anal. Bioanal. Chem.* **2018**, *410*, 7325−7336.

(18) Florindo, C.; Branco, L. C.; Marrucho, I. M. Development of Hydrophobic Deep Eutectic Solvents for Extraction of Pesticides from Aqueous Environments. *Fluid Phase Equilib.* **2017**, *448*, 135−142.

(19) Dietz, C. H. J. T.; Kroon, M. C.; van Sint Annaland, M.; Gallucci, F. Thermophysical Properties and Solubility of Different Sugar-derived Molecules in Deep Eutectic Solvents. *J. Chem. Eng. Data* **2017**, *62*, 3633−3641.

(20) Dietz, C. H. J. T.; Erve, A.; Kroon, M. C.; van Sint Annaland, M.; Gallucci, F.; Held, C. Thermodynamic Properties of Hydrophobic Deep Eutectic Solvents and Solubility of Water and HMF in Them:

Measurements and PC-SAFT Modeling. *Fluid Phase Equilib.* **2019**, *489*, 75−82.
(21) Milker, S.; Pätzold, M.; Bloh, J. Z.; Holtmann, D. Comparison of Deep Eutectic Solvents and Solvent-free Reaction Conditions for Aldol Production. *Mol. Catal.* **2019**, *466*, 70−74.
(22) Florindo, C.; McIntosh, A. J. S.; Welton, T.; Branco, L. C.; Marrucho, I. M. A Closer Look into Deep Eutectic Solvents: Exploring Intermolecular Interactions Using Solvatochromic Probes. *Phys. Chem. Chem. Phys.* **2017**, *20*, 206−213.
(23) Celebi, A. T.; Vlugt, T. J. H.; Moultos, O. A. Structural, Thermodynamic, and Transport Properties of Aqueous Reline and Ethaline Solutions from Molecular Dynamics Simulations. *J. Phys. Chem. B* **2019**, *123*, 11014−11025.
(24) Celebi, A. T.; Vlugt, T. J. H.; Moultos, O. A. Thermal Conductivity of Aqueous Solutions of Reline, Ethaline, and Glyceline Deep Eutectic Solvents; a Molecular Dynamics Simulation Study. *Mol. Phys.* **2021**, 1876263. in press
(25) Zhekenov, T.; Toksanbayev, N.; Kazakbayeva, Z.; Shah, D.; Mjalli, F. S. Formation of Type III Deep Eutectic Solvents and Effect of Water on Their Intermolecular Interactions. *Fluid Phase Equilib.* **2017**, *441*, 43−48.
(26) Baz, J.; Held, C.; Pleiss, J.; Hansen, N. Thermophysical Properties of Glyceline-Water Mixtures Investigated by Molecular Modelling. *Phys. Chem. Chem. Phys.* **2019**, *21*, 6467−6476.
(27) Shah, D.; Mjalli, F. S. Effect of Water on the Thermo-physical Properties of Reline: An Experimental and Molecular Simulation Based Approach. *Phys. Chem. Chem. Phys.* **2014**, *16*, 23900−23907.
(28) Alizadeh, V.; Malberg, F.; Pádua, A. A. H.; Kirchner, B. Are There Magic Compositions in Deep Eutectic Solvents? Effects of Composition and Water Content in Choline Chloride/Ethylene Glycol from Ab Initio Molecular Dynamics. *J. Phys. Chem. B* **2020**, *124*, 7433−7443.
(29) Sapir, L.; Harries, D. Restructuring a Deep Eutectic Solvent by Water: The Nanostructure of Hydrated Choline Chloride/Urea. *J. Chem. Theory Comput.* **2020**, *16*, 3335−3342.
(30) Kumari, P.; Shobhna; Kaur, S.; Kashyap, H. K. Influence of Hydration on the Structure of Reline Deep Eutectic Solvent: A Molecular Dynamics Study. *ACS Omega* **2018**, *3*, 15246−15255.
(31) Aryafard, M.; Karimi, A.; Harifi-Mood, A. R.; Minofar, B. Molecular Dynamics Simulations, Solvatochromic Parameters, and Preferential Solvation in Aqueous Solutions of Ethaline, Ethylene Glycol, and Choline Chloride. *J. Chem. Eng. Data* **2020**, *65*, 4556−4566.
(32) Venkatesan, S. S.; Huda, M. M.; Rai, N. Molecular Insights into Ionic Liquid/Aqueous Interface of Phosphonium Based Phase-separable Ionic Liquids. *AIP Adv.* **2019**, *9*, 045115.
(33) Sieffert, N.; Wipff, G. The [BMI][Tf_2N] Ionic Liquid/Water Binary System: A Molecular Dynamics Study of Phase Separation and of the Liquid-Liquid Interface. *J. Phys. Chem. B* **2006**, *110*, 13076−13085.
(34) Chaumont, A.; Schurhammer, R.; Wipff, G. Aqueous Interfaces with Hydrophobic Room-Temperature Ionic Liquids: A Molecular Dynamics Study. *J. Phys. Chem. B* **2005**, *109*, 18964−18973.
(35) Chevrot, G.; Schurhammer, R.; Wipff, G. Molecular Dynamics Simulations of the Aqueous Interface with the [BMI][PF_6] Ionic Liquid: Comparison of Different Solvent Models. *Phys. Chem. Chem. Phys.* **2006**, *8*, 4166.
(36) Ghatee, M. H.; Zolghadr, A. R. Local Depolarization in Hydrophobic and Hydrophilic Ionic Liquids/Water Mixtures: Car−Parrinello and Classical Molecular Dynamics Simulation. *J. Phys. Chem. C* **2013**, *117*, 2066−2077.
(37) Konieczny, J. K.; Szefczyk, B. Structure of Alkylimidazolium-based Ionic Liquids at the Interface with Vacuum and Water—A Molecular Dynamics Study. *J. Phys. Chem. B* **2015**, *119*, 3795−3807.
(38) Frost, D. S.; Dai, L. L. Molecular Dynamics Simulations of Nanoparticle Self-Assembly at Ionic Liquid−Water and Ionic Liquid−Oil Interfaces. *Langmuir* **2011**, *27*, 11339−11346.
(39) Pouramini, Z.; Mohebbi, A.; Kowsari, M. H. The Possibility of Cadmium Extraction to the Ionic Liquid 1-Hexyl-3-methylimidazolium Hexafluorophosphate in the Presence of Hydrochloric Acid: A Molecular Dynamics Study of the Water−IL Interface. *Theor. Chem. Acc.* **2019**, *138*, 99.
(40) Verma, R.; Mohan, M.; Goud, V. V.; Banerjee, T. Operational Strategies and Comprehensive Evaluation of Menthol Based Deep Eutectic Solvent for the Extraction of Lower Alcohols from Aqueous Media. *ACS Sustain. Chem. Eng.* **2018**, *6*, 16920−16932.
(41) Paul, N.; Naik, P. K.; Ribeiro, B. D.; Gooh Pattader, P. S.; Marrucho, I. M.; Banerjee, T. Molecular Dynamics Insights and Water Stability of Hydrophobic Deep Eutectic Solvents Aided Extraction of Nitenpyram from an Aqueous Environment. *J. Phys. Chem. B* **2020**, *124*, 7405−7420.
(42) Paul, R.; Mitra, A.; Paul, S. Phase Separation Property of a Hydrophobic Deep Eutectic Solvent−Water Binary Mixture: A Molecular Dynamics Simulation Study. *J. Chem. Phys.* **2021**, *154*, 244504.
(43) Doherty, B.; Zhong, X.; Gathiaka, S.; Li, B.; Acevedo, O. Revisiting OPLS Force Field Parameters for Ionic Liquid Simulations. *J. Chem. Theory Comput.* **2017**, *13*, 6131−6145.
(44) Cui, K.; Yethiraj, A.; Schmidt, J. R. Influence of Charge Scaling on the Solvation Properties of Ionic Liquid Solutions. *J. Phys. Chem. B* **2019**, *123*, 9222−9229.
(45) Mainberger, S.; Kindlein, M.; Bezold, F.; Elts, E.; Minceva, M.; Briesen, H. Deep Eutectic Solvent Formation: A Structural View Using Molecular Dynamics Simulations with Classical Force Fields. *Mol. Phys.* **2017**, *115*, 1309−1321.
(46) Salehi, H. S.; Celebi, A. T.; Vlugt, T. J. H.; Moultos, O. A. Thermodynamic, Transport, and Structural Properties of Hydrophobic Deep Eutectic Solvents Composed of Tetraalkylammonium Chloride and Decanoic Acid. *J. Chem. Phys.* **2021**, *154*, 144502.
(47) Perkins, S. L.; Painter, P.; Colina, C. M. Molecular Dynamic Simulations and Vibrational Analysis of an Ionic Liquid Analogue. *J. Phys. Chem. B* **2013**, *117*, 10250−10260.
(48) Salehi, H. S.; Hens, R.; Moultos, O. A.; Vlugt, T. J. H. Computation of Gas Solubilities in Choline Chloride Urea and Choline Chloride Ethylene Glycol Deep Eutectic Solvents Using Monte Carlo Simulations. *J. Mol. Liq.* **2020**, *316*, 113729.
(49) Wang, J.; Wolf, R. M.; Caldwell, J. W.; Kollman, P. A.; Case, D. A. Development and Testing of a General Amber Force Field. *J. Comput. Chem.* **2004**, *25*, 1157−1174.
(50) Fox, T.; Kollman, P. A. Application of the RESP Methodology in the Parametrization of Organic Solvents. *J. Phys. Chem. B* **1998**, *102*, 8070−8079.
(51) Bayly, C. I.; Cieplak, P.; Cornell, W.; Kollman, P. A. A Well-behaved Electrostatic Potential Based Method Using Charge Restraints for Deriving Atomic Charges: The RESP Model. *J. Phys. Chem.* **1993**, *97*, 10269−10280.
(52) Frisch, M. J.; Trucks, G. W.; Schlegel, H. B.; Scuseria, G. E.; Robb, M. A.; Cheeseman, J. R.; Scalmani, G.; Barone, V.; Mennucci, B.; Petersson, G. A.; et al. *Gaussian 09*, Revision B.01; Gaussian, Inc.: Wallingford CT, 2010.
(53) Dupradeau, F.-Y.; Pigache, A.; Zaffran, T.; Savineau, C.; Lelong, R.; Grivel, N.; Lelong, D.; Rosanski, W.; Cieplak, P. The R.E.D. Tools: Advances in RESP and ESP Charge Derivation and Force Field Library Building. *Phys. Chem. Chem. Phys.* **2010**, *12*, 7821−7839.
(54) Xin, K.; Roghair, I.; Gallucci, F.; van Sint Annaland, M. Total Vapor Pressure of Hydrophobic Deep Eutectic Solvents: Experiments and Modelling. *J. Mol. Liq.* **2021**, *325*, 115227.
(55) Bergua, F.; Castro, M.; Muñoz-Embid, J.; Lafuente, C.; Artal, M. Hydrophobic Eutectic Solvents: Thermophysical Study and Application in Removal of Pharmaceutical Products from Water. *Chem. Eng. J.* **2021**, *411*, 128472.
(56) Allen, M. P.; Tildesley, D. J. *Computer Simulation of Liquids*, 2nd ed.; Oxford University Press, Inc.: New York, NY, USA, 2017.
(57) Berendsen, H. J. C.; Grigera, J. R.; Straatsma, T. P. The Missing Term in Effective Pair Potentials. *J. Phys. Chem.* **1987**, *91*, 6269−6271.
(58) Ryckaert, J.-P.; Ciccotti, G.; Berendsen, H. J. C. Numerical Integration of the Cartesian Equations of Motion of a System with

Constraints: Molecular Dynamics of *n*-Alkanes. *J. Comput. Phys.* **1977**, *23*, 327−341.
(59) Frenkel, D.; Smit, B. *Understanding Molecular Simulation: From Algorithms to Applications*, 2nd ed.; Academic Press: San Diego, California, 2002; Vol. *1*.
(60) Verlet, L. Computer "Experiments" on Classical Fluids. I. Thermodynamical Properties of Lennard-Jones Molecules. *Phys. Rev.* **1967**, *159*, 98−103.
(61) Swope, W. C.; Andersen, H. C.; Berens, P. H.; Wilson, K. R. A Computer Simulation Method for the Calculation of Equilibrium Constants for the Formation of Physical Clusters of Molecules: Application to Small Water Clusters. *J. Chem. Phys.* **1982**, *76*, 637−649.
(62) Plimpton, S. Fast Parallel Algorithms for Short-Range Molecular Dynamics. *J. Comput. Phys.* **1995**, *117*, 1−19.
(63) Martínez, L.; Andrade, R.; Birgin, E. G.; Martínez, J. M. PACKMOL: A Package for Building Initial Configurations for Molecular Dynamics Simulations. *J. Comput. Chem.* **2009**, *30*, 2157−2164.
(64) Humphrey, W.; Dalke, A.; Schulten, K. VMD: Visual Molecular Dynamics. *J. Mol. Graph.* **1996**, *14*, 33−38.
(65) Isele-Holder, R. E.; Mitchell, W.; Ismail, A. E. Development and Application of a Particle-Particle Particle-Mesh Ewald Method for Dispersion Interactions. *J. Chem. Phys.* **2012**, *137*, 174107.
(66) Isele-Holder, R. E.; Mitchell, W.; Hammond, J. R.; Kohlmeyer, A.; Ismail, A. E. Reconsidering Dispersion Potentials: Reduced Cutoffs in Mesh-based Ewald Solvers Can Be Faster Than Truncation. *J. Chem. Theory Comput.* **2013**, *9*, 5412−5420.
(67) Jamali, S. H.; Wolff, L.; Becker, T. M.; de Groen, M.; Ramdin, M.; Hartkamp, R.; Bardow, A.; Vlugt, T. J. H.; Moultos, O. A. OCTP: A Tool for On-the-Fly Calculation of Transport Properties of Fluids with the Order-*n* Algorithm in LAMMPS. *J. Chem. Inf. Model.* **2019**, *59*, 1290−1294.
(68) Papavasileiou, K. D.; Moultos, O. A.; Economou, I. G. Predictions of Water/Oil Interfacial Tension at Elevated Temperatures and Pressures: A Molecular Dynamics Simulation Study with Biomolecular Force Fields. *Fluid Phase Equilib.* **2018**, *476*, 30−38.
(69) Luzar, A.; Chandler, D. Effect of Environment on Hydrogen Bond Dynamics in Liquid Water. *Phys. Rev. Lett.* **1996**, *76*, 928−931.
(70) Zhao, W.; Leroy, F.; Heggen, B.; Zahn, S.; Kirchner, B.; Balasubramanian, S.; Müller-Plathe, F. Are There Stable Ion-Pairs in Room-Temperature Ionic Liquids? Molecular Dynamics Simulations of 1-*n*-Butyl-3-methylimidazolium Hexafluorophosphate. *J. Am. Chem. Soc.* **2009**, *131*, 15825−15833.
(71) Kohagen, M.; Brehm, M.; Lingscheid, Y.; Giernoth, R.; Sangoro, J.; Kremer, F.; Naumov, S.; Iacob, C.; Kärger, J.; Valiullin, R.; Kirchner, B. How Hydrogen Bonds Influence the Mobility of Imidazolium-based Ionic Liquids. A Combined Theoretical and Experimental Study of 1-*n*-Butyl-3-methylimidazolium Bromide. *J. Phys. Chem. B* **2011**, *115*, 15280−15288.
(72) Martins, M. A. R.; Crespo, E. A.; Pontes, P. V. A.; Silva, L. P.; Bülow, M.; Maximo, G. J.; Batista, E. A. C.; Held, C.; Pinho, S. P.; Coutinho, J. A. P. Tunable Hydrophobic Eutectic Solvents Based on Terpenes and Monocarboxylic Acids. *ACS Sustain. Chem. Eng.* **2018**, *6*, 8836−8846.
(73) van Osch, D. J. G. P.; Dietz, C. H. J. T.; van Spronsen, J.; Kroon, M. C.; Gallucci, F.; van Sint Annaland, M.; Tuinier, R. A Search for Natural Hydrophobic Deep Eutectic Solvents Based on Natural Components. *ACS Sustain. Chem. Eng.* **2019**, *7*, 2933−2942.

https://doi.org/10.1021/acs.jpcb.1c07796
J. Phys. Chem. B 2021, 125, 12303−12314